NfoR, Chromate Reductase or FMN reductase ?

Audrey G. O'Neill, Brett A. Beaupre, Yuanzhang Zheng, Dali Liu and Graham R. Moran[†]

Department of Chemistry and Biochemistry, 1068 W Sheridan Rd, Loyola University Chicago, Chicago, IL 60660.

[†]Corresponding author; phone: (773)508-3756; email: gmoran3@luc.edu

This research was supported by National Science Foundation Grant 1904480 to G.R.M. and Dr. Michael and Dorothy Carbon Fellowships to A.G.O.

RUNNING TITLE: NfoR is an FMN reductase

Abstract

Soil bacteria can detoxify Cr(VI) ions by reduction. Within the last two decades numerous reports of chromate reductase enzymes have been published. These reports purport catalytic reduction of chromate ions by specific enzymes. These enzymes each have sequence similarity to known-redox active flavoproteins. We investigated the enzyme NfoR from Staphlococcus aureus that was claimed to be upregulated in chromate rich soils and to have chromate reductase activity (Han H, Ling Z, Zhou T, Xu R, He Y, Liu P, Li X. 2017. Sci Rep 7:15481.). We show that NfoR has structural similarity to known FMN reductases and reduces FMN as a substrate. NfoR binds FMN with a dissociation constant of 0.4 μM. The enzyme then binds NADPH with a dissociation constant of 140 μM and reduces the flavin at a rate of 1350 s^{-1}. Turnover of the enzyme is apparently limited by the rate of product release that occurs with a net rate constant of 0.45 s^{-1}. The rate of product release limits the rate of observed chromate reduction, so the net rate of chromate reduction by NfoR is orders of magnitude slower than this process occurs in solution. We propose that NfoR is an FMN reductase and that the criterium required to define chromate reduction as enzymatic has not been met. That NfoR expression is increased in the presence of chromate suggests that the survival adaption was to increase the net rate of chromate reduction by facile, adventitious redox processes.

Importance

Chromate is a toxic byproduct of multiple industrial processes. Chromate reduction is an important biological activity that ameliorates Cr(VI) toxicity. Numerous researchers have claimed chromate reductase activity by observing chromate reduction. However, all claimed chromate reductase enzymes have flavin as a cofactor or use a flavin as a substrate. We show here that NfoR, an enzyme claimed to be a chromate reductase, is in fact an FMN reductase. In addition, we show that reduction of a flavin is a viable way to transfer electrons to chromate, but that it is unlikely to be the native function of enzymes. We propose that upregulation of a redox active flavoprotein is a viable means to detoxify chromate that relies on adventitious reduction that is not catalyzed.

Introduction

Hexavalent chromium pollution in the environment poses considerable health risks. Chromium is widely used in industrial processes such as the manufacturing of alloys, paints, paper, and tanning (1). The waste produced is often improperly disposed of and used as fill material on construction sites and wetlands, and as a result, the toxic Cr(VI) enters and contaminates the surrounding soil and water. Chromium can enter the human body via absorption through skin, ingestion, or inhalation. Compounds of Cr(VI) such as chromate are soluble, toxic and mutagenic, with long-term exposure leading to ulceration, liver failure, and skin disorders, and ultimately lung and digestive tract cancer (2). In contrast, compounds of Cr(III) are non-mutagenic, less toxic, and insoluble(3). As such, chromate pollution can be remediated through the reduction of Cr(VI) to Cr(III). However, the implementation of such processes in effected areas can be prohibitively expensive and causes further disruption to the environment (4).

Bioremediation is a natural, non-destructive phenomenon that nullifies chromate pollution (3, 5). Several enzymes have been identified as possible candidates for the bioremediation of hexavalent chromium, though most have been characterized as also having functions other than chromate reduction, such as nitroreductases, quinone reductases, and flavin reductases (4). Strains of chromate-resistant *Staphylococcus aureus* were found to upregulate the expression of an NAD(P)H-flavin oxidoreductase (NfoR), and preliminary research suggested that NfoR functions as a chromate reductase and nitroreductase with enhanced activity in the presence of Cu(II) (6). Here we show that NfoR functions as an FMN-reductase, rapidly reducing bound FMN followed by rate limiting release of $FMNH_2$. We submit that NfoR is

not a chromate reductase and instead propose that through selection for upregulation of NfoR expression, the bacteria have acquired a modest adaptation in response to the environment that accomplishes chromate detoxification. This modification increases production of reduced flavin, a molecule capable of reducing a plethora of harmful oxidants. We also submit that the designation of an enzyme as a chromate reductase must be accompanied by a formal demonstration of rate enhancement, and that evidence of chromate reduction by itself is insufficient to establish this category of enzymatic activity.

Materials and Methods

Materials, quantitation and reaction conditions: Tris(hydroxymethyl)aminomethane (Tris), sodium dihydrogen phosphate, ethylenediaminetetraacetic acid (EDTA), kanamycin, isopropyl β-D-1-thiogalactopyranoside (IPTG), HEPES buffer, Urea, NaCl, potassium bromide, BD TALON affinity column packing, the Miller formulation of lysogeny broth (LB) powder, and potassium bromide were purchased from Fisher Scientific. Reduced nicotinamide adenine dinucleotide phosphate (NADPH) was purchased from RPI Research Products. Dextrose powder was from Spectrum Chemical. Riboflavin 5'-monophosphate (FMN) and glucose oxidase were obtained from Sigma-Millipore. Streptomycin sulfate powder was made by Gibco. Imidazole and glycerol were acquired from Acros Organics. Competent *Escherichia coli* BL21 DE3 cells were purchased from New England Biolabs. Copper(II) chloride, copper(II) sulfate and potassium dichromate were from VWR. All concentrations of substrates and products were determined spectrophotometrically using known extinction coefficients: (NAD(P)H; ε_{340} = 6,220 $M^{-1}cm^{-1}$, $NAD(P)^+$; ε_{260} = 17,800 $M^{-1}cm^{-1}$, FMN; ε_{450} = 12,200 $M^{-1}cm^{-1}$, FAD; ε_{450} = 11,300 $M^{-1}cm^{-1}$, NfoR; ε_{280} = 31,000 $M^{-1}cm^{-1}$). All kinetic experiments were undertaken in assay buffer (20 mM Tris, 100 mM NaCl, pH 8.0) at 20 ^{o}C

***Plasmid expression construct*:** Plasmid was kindly provided by Dr. Xiangkai Li's group at Lanzhou University. Briefly, the *nfoR* gene was amplified using oligonucleotides that incorporated both Nco I restriction site and 6 x His tag to the N-terminus (*nfoR*-F CCCATGGGCCATCATCATCATCATCAC-ATGAGCAATATGAATCAAACAATTAT) and Xho I restriction to the C-terminus (*nfoR*-R CCGCTCGAGTTCTTTTGGTCCAACCCATT). The amplified gene was then

digested and cloned into the Nco I and Xho I sites of pET28a yielding an expression construct (named here as pSanfoR) with the *nfoR* gene fused to 6 x His tags at both the N-terminus and C-terminus.

***Production and Purification of NfoR*:** BL21(DE3) cells harboring the pSanfoR plasmid were prepared as cell stocks by selecting a single colony from transformation plates and inoculating 20 mL of LB medium with kanamycin selection (50 µg/mL). The cells were grown until early exponential phase at which time sterilized glycerol was added to 20 %, and 1 mL aliquots were frozen at -80 °C. To express NfoR, a 50 mL starter culture of LB medium containing kanamycin (50 µg/mL) was inoculated with the frozen glycerol cell stock cells and grown overnight at 37 °C with shaking at 250 rpm. This culture was used to inoculate 2 x 1 L of sterile LB medium with kanamycin (50 µg/mL). The cultures were grown at 37 °C and shaken at 250 rpm until reaching an OD_{600} ~ 0.6. The cultures were cooled on ice at 4 °C for 40 minutes before inducing with IPTG (0.5 mM). Cultures were then incubated at 16 °C and shaken at 200 rpm for 20 hours. Cells were harvested by centrifugation at 6,370 x g for 20 min. The cell pellet was resuspended in buffer A (10 mM imidazole, 500 mM NaCl, 50 mM NaH_2PO_4, pH 7.5) and lysed while on ice by sonication with a QSonica Q500 sonicator at 30% amplitude for 7 min. Cell debris was pelleted and the supernatant retained by centrifuging twice at 31,000 x g for 20 min with decanting between. The supernatant was then subjected to Ni^{2+} affinity chromatography using two 5 mL HisTrap FF columns connected in series and pre-equilibrated with buffer A. NfoR was eluted with a 20-column volume linear gradient of imidazole (10 mM to 500 mM) in buffer A. Fractions containing NfoR were identified by SDS-PAGE correlated to the 280 nm chromatogram, and were pooled together and exchanged

into gel filtration buffer (50 mM HEPES, 300 mM NaCl, pH 7.5) using 10 KDa Amicon ultra centrifugal filters (Millipore). The pooled and concentrated sample (2 mL) was subject to size exclusion chromatography using a HiLoad 16/60 (16 mm x 60 cm) Superdex column (GE Healthcare) equilibrated in gel filtration buffer. The fractions of the dominant elution peak were pooled. Protein concentrations were measured by UV absorption at 280 nm based on the calculated extinction coefficient $\varepsilon_{280} = 3.1 \times 10^4\ M^{-1}\ cm^{-1}$ (7).

Apo-NfoR was prepared according to a modified protocol via His-tagged based immobilization as described previously (8). Briefly, a 5 mL HisTrap FF column was pre-equilibrated with buffer B (10 mM imidazole, 300 mM NaCl, 50 mM HEPES, pH 7.5), and 20 mL of 20 µM of pure NfoR was loaded onto the column. The bound protein was washed with 10 column-volumes of a mild denaturant (2 M KBr, 2 M Urea, dissolved in buffer B). NfoR was then eluted with a 20-column volume linear imidazole gradient (10-250 mM imidazole) in buffer B. Apo-NfoR was then exchanged into assay buffer (20 mM Tris, 100 mM NaCl, pH 8.0) using centrifugal concentrators.

Transient State FMN reduction: The hydride transfer reaction from NADPH to FMN was observed at 450 nm using rapid mixing methods. NfoR (12.5 µM) was prepared anaerobically in a tonometer in assay buffer that included 1 mM dextrose and 25 µM FMN. The tonometer was made anaerobic using published protocols (9). Once the exchange of dissolved gases was complete, glucose oxidase was added from the tonometer side arm to provide 1 U/mL of activity. The tonometer was then mounted onto a Hitech DX2 (TgK Scientific) stopped-flow spectrophotometer equipped with ceramic valves and a PEEK flow circuit. NADPH solutions were prepared in the same buffer with 1 mM dextrose and sparged with purified argon gas for five

minutes. Glucose oxidase was then added to 1 U/mL and the syringe was captured and mounted to the stopped-flow instrument. The reduction of FMN was observed for two time-frames. Initial rapid hydride transfer was observed for one second. For NADPH concentrations in excess of the enzyme concentration, subsequent net FMN reduction was observed for 200 seconds. The dependence of the rate of the initial hydride transfer was modelled using KinTek Explorer software to the model depicted in Figure 1. This model assumes that the binding affinity of NfoR for FMN is sufficiently high that the NfoR-FMN equilibrium need not be considered. As such the fit returns estimates of both the (NfoR•FMN)•NADPH dissociation constant and the limiting rate of hydride transfer. Data that covered 200 seconds were fit to a linear combination of two exponentials as described by Equation 1, where the first phase ($\Delta Abs_1 e^{-k_{obs1}t}$) accounts for the tail end of the initial hydride transfer that is observed in these data between 0.01-0.1 seconds. In the second phase k_{obs2} is the observed rate constant, ΔAbs_2 is the associated amplitude of the absorption change and C is the Abs_{450nm} endpoint.

Equation 1. $$Abs_{450nm} = \Delta Abs_1 e^{-k_{obs1}t} + \Delta Abs_2 e^{-k_{obs2}t} + C$$

Enzyme Activity Assays: Routine activity measurements of purified NfoR were made by monitoring consumption of NADPH at 25 °C. In 1 mL of assay buffer, 4 µM NfoR supplemented with 200 µM flavin mononucleotide (FMN) was mixed with 200 µM NADPH. The reaction was monitored at 340 nm ($\Delta\varepsilon_{340} = 6.22 \times 10^3\ M^{-1}\ cm^{-1}$) using a Shimadzu 2600 spectrophotometer and the reaction rate was calculated from a fit to the linear portion of the progress curve between 5 and 20 seconds.

A comparison of the kinetic behavior of NfoR in the presence and absence of a sacrificial oxidant was carried by observing the turnover of the enzyme under aerobic and anaerobic conditions. The aerobic reaction included 1 μM NfoR with 5 μM FMN and was observed reacting with a range of NADPH concentrations (20, 40, 60, 80, 100, 120 μM) in the presence of atmospheric dioxygen (~250 μM) at 340 nm using a Shimadzu 2600 spectrophotometer.

Anaerobic turnover was observed using published protocols for anaerobiosis with stopped-flow instrumentation (9). NfoR (1 μM) was prepared in assay buffer in a tonometer in the presence of 300 μM NADPH and 1 mM dextrose. Once anaerobic, glucose oxidase to 1 U/mL was added from the tonometer sidearm and mounted onto the stopped-flow instrument. The NfoR/NADPH solution was then mixed with a range of FMN concentrations (15.4, 16.4, 18.4, 22 μM) and the reaction was observed at 450 nm.

The anaerobic and aerobic data sets obtained were fit simultaneously to the model depicted in Figure 2 using numerical integration subroutines implemented in KinTek Explorer software (KinTeK Corp.). In this scheme the hydride transfer rate constant was fixed to the value determined from the transient state observation of hydride transfer described above. The bimolecular rate constant for reduced flavins reacting with dioxygen was fixed to the known value of 250 $M^{-1}s^{-1}$ for this reaction (10). In addition, the rate constants that define the NfoR•FMN dissociation constant were fixed to a ratio that equals the dissociation constant determined by perturbation of the FMN fluorescence spectrum (see below).

FMN Equilibrium Binding: The dissociation constant for the NfoR•FMN complex was estimated from perturbation of the FMN emission spectrum when titrated with NfoR. Near apo-NfoR was

prepared as described above. For each ratio of FMN to NfoR, 2,950 µL of 3 µM FMN in assay buffer was placed in a 3 mL fluorescence cuvette and a 50 µL addition of two-fold serially diluted NfoR stocks was added. For each NfoR concentration, an emission spectrum was recorded using a Shimadzu RF6000 spectrofluorometer. Formation of the NfoR•FMN complex was registered as a decrease in the area of the FMN emission spectrum from 460-600 nm when excited at 450 nm. The change in intensity at 530 nm was plotted against the concentration of added NfoR. The data were fit to the solution of the quadratic form of the single site binding equation added to a straight line (Equation 2). The m[NfoR] term is to account for what is assumed to be a fluorescence contribution from residual FMN in the NfoR sample (11).

Equation 2. $$[\mathrm{NfoR} \bullet \mathrm{FMN}] = \frac{([\mathrm{FMN}]+[\mathrm{NfoR}]+ \mathrm{K}_{FMN})-\sqrt{([\mathrm{FMN}]+[\mathrm{NfoR}]+ \mathrm{K}_{\mathrm{FMN}})^2-4([\mathrm{FMN}]+[\mathrm{NfoR}])}}{2} + m[NfoR]$$

Crystallization and Structure Determination: The NfoR•FMN•NAD^+ complex was crystallized by the sitting drop, vapor diffusion method. Drops were formed at room temperature by mixing 6 µL of 45 mg/mL of purified NfoR with 10 mM NAD^+ in 50 mM HEPES, 300 mM NaCl, pH 7.5 with 6 µL of 30% PEG 4000, 210 mM ammonium acetate, and 100 mM sodium citrate, pH 5.6. Initial crystals appeared in 14 days and were used to seed subsequent crystal growth that grew within 7 days. The crystals grew to a size of approximately 400 x 400 x 400 µm. Crystals were cryo-protected for data collection by soaking briefly in the well solution supplemented with glycerol to 20%. Crystals were then flash-cooled by plunging in liquid nitrogen.

Diffraction data were collected at 100 K at the Structural Biology Center beamline 19-BM of the Advanced Photon Source at Argonne National Laboratory. The beamline was equipped

with an ADSC-315r detector. Data were collected using an oscillation angle of 0.5° over a range of 180° and an exposure time of 1 second per frame. The wavelength was fixed at 0.97856 Å. Diffraction images were processed using HKL2000(12). Data processing statistics are given in Table 1. Phasing was conducted via molecular replacement using program phaser. A homologous model of the putative NAD(P)H-flavin oxidoreductase from *Streptococcus pyogenes* M1 GAS was used as a starting search model (PDB ID: 2HAY). The model building and refinement was undertaken in Coot (13) and Phenix (14) respectively in a repeated manner until the lowest R_{free} was achieved. The coordinates and structure factors have been deposited in the Protein Data Bank with accession code 7JH4. Structural analysis and figures are made using PyMOL (The PyMOL Molecular Graphics System, Version 2.0 Schrödinger, LLC.).

Reoxidation of Flavins by Chromate and Copper: In order to establish if the reduction of metal ions by NfoR is catalytic, the rate of reduction in the presence of the enzyme was compared to the rate in solution using anaerobic double mixing stopped flow spectrophotometry. NfoR (10 µM final) with FMN (100 µM final) was mixed with NADPH (12 µM final) in a range of concentrations of cupric copper (0, 3, 12.5, 25, 100, 200 µM) or chromate (0, 6.26, 12.5, 50, 100, 200 µM) and observed at 450 nm for 5 or 10 seconds respectively.

As controls, anaerobic FAD in a tonometer (10 µM final) in assay buffer was photoreduced in the presence of 1 mM methionine using a Xenon arc lamp (15). The reduced flavin was then mixed with oxidant (40, 80, 160, 320, 640 µM $CuSO_4$ or 40, 80, 320, 640 µM K_2CrO_4 and observed at 450 nm using CCD detection. FAD was used in these measurements to avoid the complication arising from the propensity of FMN to decompose when irradiated (11). The control data were

fit to a single exponential phase according to Equation 3. In this equation ΔAbs_{450nm} is the change in absorption at 450 nm, k_{obs} is the observed rate constant for $FADH_2$ oxidation and C is the endpoint absorption at 450 nm.

Equation 3 $$Abs_{450nm} = \Delta Abs_{450nm}(e^{-k_{obs}t}) + C$$

Results

***Expression and Purification of NfoR*:** NfoR was expressed and purified to yield 45 mg of protein per liter of culture. The enzyme proved to be moderately unstable often precipitating with routine manipulations. The addition of 100 mM NaCl improved tractability sufficiently to permit characterization. The as isolated enzyme typically copurified with a ~17 % fractional content of FMN indicating non-covalent but high affinity binding for the FMN substrate. The copurified FMN could be removed by immobilization on a nickel affinity column in the presence of denaturants. Both the FMN-bound and apo-form of NfoR could be concentrated and stored indefinitely at -80 °C without appreciable loss of activity. The turnover number of the enzyme under anaerobic conditions in the presence of saturating substrates (300 µM NADPH, 150 µM FMN) is 0.45 s^{-1}.

Transient State FMN reduction: The two-electron reduction of FMN results in a decrease in the intensity of absorption of the isoalloxazine from 340-520 nm. This signal was used to observe hydride transfer from NADPH to the FMN on the surface of NfoR. NfoR in the presence of FMN (twice the enzyme concentration) was mixed with NADPH and observed at 450 nm (Figure 1). NADPH concentrations in excess of the enzyme and equivalent to or greater than the FMN concentration yielded two phases of reduction. The rate of the first phase titrated with NADPH concentration to a limit, indicating that reduction involves pre-equilibrium formation of an NfoR•FMN•NADPH complex that is followed by hydride transfer. Global fitting using numerical integration returned a ratio for the association and dissociation rate constants for NADPH binding that gave a K_{NADPH} of 141 ± 5 µM. A confidence interval analysis of the fit revealed that the ratio of these rates (equilibrium constant) is well-described by the data, but that the actual magnitude

of the rate constants for binding are not confined well. The fit also provided a measure of the rate constant for hydride transfer at 1350 ± 20 s^{-1} (Figure 1A). These data indicate both rapid NADPH binding and hydride transfer to FMN in NfoR. The subsequent phase observed was the reduction of the excess FMN and was largely independent of the concentration of NADPH and occurred with an average rate constant of 0.034 ± 0.005 s^{-1} (Figure 1B). This rate is not assigned to an instrinsic rate for any specific step in catalysis as it is more than 10-fold slower than the NfoR turnover number. The slow relative rate observed is likely a function of the limiting concentration of FMN present or the trapping of the enzyme in an inhibitory product complex (Eg. NfoR•FMNH2•NADPH) in which the release of $FMNH_2$ and/or NADPH is slow.

The Effect of an External Oxidant on the NfoR Steady State: The kinetic behavior of NfoR in the presence and absence of a external oxidant was demonstrated by conducting activity assays under aerobic and anaerobic conditions. Aerobic activity was monitored at 340 nm in the presence of atmospheric dioxygen (~250 µM); at low enzyme concentration this wavelength principally reports the two-electron oxidation of NADPH. Aerobic activity assays were carried out in the presence of limiting FMN (5 µM, 5-fold excess relative to the NfoR concentration) and reacted with NADPH concentrations that ranged from 20 to 120-fold greater than the enzyme concentration (1 µM). In each assay the rate of NADPH consumption is constant and does not abate until all NADPH is consumed (Figure 4A). Assays of this type may be interpreted as exceedingly tight binding for NADPH. However, the transient state observation of the dependence of the rate of hydride transfer indicated that the binding energy for the (NfoR•FMN)•NADPH complex is modest at ~140 µM (Figure 1). Moreover, the fact that

consumption of NADPH is greater than the available FMN concentration, dictates that FMN is regenerated in the reaction. As such these traces are interpreted as the activity of NfoR in the presence of a constant concentration of FMN that is maintained by reoxidation.

Under anaerobic conditions the reduction of FMN as observed at 450 nm is curving and asymptotic consistent with the progressive exhaustion of substrate(s) (Figure 4B); neither of which are regenerated in the reaction. As a demonstration of concept, the data for aerobic and anaerobic assays were fit globally to the same model (Figure 2) where the principal difference was that the dioxygen concentration was set to zero for the anaerobic data set. While progress curves cannot be fit to reliably determine microscopic rate constants the fit makes the case that an external oxidant will promote the net chemistry of NfoR and promoting to the erroneous conclusion that the external oxidant is a substrate.

FMN Equilibrium Binding: The association of FMN to oxidized apo-NfoR results in a perturbation of the FMN fluorescence spectrum when excited with 450 nm light and provides a means to measure the dissociation constant for the NfoR•FMN complex. The data obtained indicated that FMN has high affinity for the oxidized enzyme with a K_d of 440 ± 37 nM (Figure 5). This is in good agreement with the data from anaerobic transient state experiments where the reduction of NfoR•FMN by NADPH is independent of the concentration of FMN.

The Structure of NfoR: NfoR crystallized using vapor diffusion, sitting drop to yield rhombic crystals that diffracted to a limit of 2.02 Å with the C2 space group (Table 1). The topology of the NfoR enzyme closely resembles the paradigm FMN reductase, NfsA from *Vibrio harveyi* (PDB ID:

2BKJ) that serves to reduce the flavin substrate of luciferase(16)(Figure 6). When compared directly with the NfsA structure using the CEalign command available in Pymol software (Schrödinger Inc), the RMSD value for 176/240 residues was 3.69 Å. This modest level of structural similarity is in accord with the low level of sequence identity (19 %) obtained from Clustal Omega alignment of the primary structures (Grey shading in Figure 7). Two topological differences are apparent in the secondary structure comparison of NfsA and NfoR. These differences are summarized in topology diagrams in Figure 6, and show that the two subunits of both structures are entwined with secondary structural elements from both protomers to form functional domains. Two of the C-terminal secondary elements that interact with the other protomer in this manner in NfsA are absent from the NfoR structure and this structure is therefore truncated relative to NfsA. In addition, NfoR has no helix between residues 180 and 186, while NfsA has a helix at this part of the structure that spans residues 136-143. NfoR also has an additional helix that is formed between residues 110 and 127. Positionally, this helix is in a similar position to two helices in NfsA that arise between residues 212 and 235.

The FMN binding site of NfoR has broad features similar to that found in NfsA (Figure 7). However, after careful analysis, we have determined that a reduced FMN (FNR) has been generated during data collection as a radiation-induced artifact (17). The bent FMN ring more faithfully fits to the observed density, and does not generate any residual difference density (Fo-Fc). When oxidized FMN was fit, the R_{free} was notably worse by ~0.5 percent, and the difference density also suggests the ring was bent. A number of previously published papers have documented this X-ray induced artifact (18, 19).

Only the density for the nicotinamide of the NAD^+ was observed in the map its positioning would suggest that it is likely to be a crystallographic artifact. Among five subunits in an asymmetric unit of the space group C2, the nicotinamide ring of the NAD^+ can only be observed in two subunits. The observation of the electron density of the nicotinamide ring in the active site is strictly accompanied by a specific inter-subunit interaction in the vicinity, which is a π-π/π-cation interaction between W70 and R103 from an adjacent subunit in the crystallographic lattice (Figure S1). When W70 is not interacting with R103, the nicotinamide ring was not observed in the active site due to hinderance caused by W70 in a different orientation. We speculate that W70 plays a role in NADH binding and NAD^+ release. Since the observation of nicotinamide ring is strictly related to this interaction that only exists in crystals, the complex structure we observed here is a result of soaking after the crystals are formed.

Moreover, the position of the nicotinamide ring is not optimal for hydride transfer. While the distance to the flavin is typical for such complexes (3.5 Å) (20), the nicotinamide is roughly 90 degrees rotated (anticlockwise in Figure 7) from the position expected for reduction (20). The residues shown in Figure 7 that surround the FMN substrate are shown for reference and are not a complete set of interacting residues with this ligand. Cupric ions have been proposed to have a modulating influence on the reduction of chromate (6). It is of note that repeated attempts to co-crystallize NfoR with copper ions failed to reveal a copper binding site to the enzyme, even at millimolar concentrations of the metal ion (see below).

Reoxidation of Flavins by Chromate and Copper: To ascertain catalysis with respect to NfoR and the reduction of chromate or other metal ions, NfoR with FMN was mixed with one of two oxidant

metal ions in the presence of NADPH under anaerobic conditions. The primary objective was to establish if NfoR can reduce metal ions more rapidly than they reduce in solution in the presence of reduced flavin. Figure 9A depicts the reoxidation of $FMNH_2$ generated by NfoR reacting with chromate ions. The data show qualitatively that reduction of chromate is contingent on the release of $FMNH_2$ from the enzyme in that a significant lag corresponding in time to the inception of product release (cf. Figure 3B and 9A). In contrast, the data shown in Figure 9B indicate that cupric ions can access and oxidize $FMNH_2$ prior to release from the enzyme. These outcomes are likely to reflect the accessibility of the reduced flavin to the form of the metal ion presented, in that the radius of copper ions is smaller (and similar to that of dioxygen) than that of chromate (1.4 Å vs 2.5 Å).

The reduction of chromate or copper(II) ions by $FMNH_2$ derived from NfoR is orders of magnitude slower than it occurs in solution in the presence of unliganded $FADH_2$. These data are less complex than the those dependent on the kinetics of NfoR and are described well when fit to a single exponential phase. Based on the data acquired the rate constants for reduction of chromate and copper by $FADH_2$ are estimated to be 1.0×10^4 and 6.4×10^5 $M^{-1}s^{-1}$ respectively (Figure 10). The control data for chromate have added complexity. The dependence has a positive intercept suggesting a complex between the Cr VI compound and the $FADH_2$ (Figure 10B inset). While an encompassing kinetic model accounting for this has not been developed, it is reasonably explained in broad terms by the known tendency of chromate to associate with nucleotides (21-24). These data definitively establish that NfoR does not catalyze reduction of copper(II) or chromate ions as the rates observed with reduced flavin at millimolar concentrations are respectively 1400- and 22-fold more rapid than the apparent turnover number of NfoR ($0.45\ s^{-1}$).

The use of copper in this instance relates to the claim that NfoR chromate reducing activity is enhanced in the presence of copper ions(6). These data show that copper is, from a kinetic standpoint, a more effective oxidant than chromate for $FMNH_2$ derived from NfoR, and any observed rate enhancement in terms of NADPH consumption is a function of that propensity and not a result of modulation by binding.

Discussion

Chromium is a hazardous biproduct/pollutant produced by industrial processes (2, 3). One strategy for remediation of contaminated soils and water is to reduce toxic soluble chromium VI compounds to the less toxic and insoluble chromium III oxides and hydroxides. In 1994, Losi et al., demonstrated that irrigation of agricultural soils with chromate laced water resulted in a 20-fold diminishment of soluble chromium in water outflow. The conclusion was that bacteria in the soil possess strategies to ameliorate chromium toxicity (5). Early reports of bacterial chromium reduction described the efficiency of flavin reductases in the reduction of chromium and emphasized the facile thermodynamics and kinetics of this reaction (25). Importantly, this initial report did not describe the enzymes involved as chromium (or chromate) reductases. However, in the same year it was claimed that *Vibrio harveyi* nitroreductase (formally a flavin reductase) was also a chromate reductase, without demonstrating catalytic or enzymological characteristics that definitively support such a claim (26). Shortly after Ackerley et al., was one of the first to identify proteins long regarded as flavin reductases as chromate reductase enzymes. These researchers identified ChrR from *P. putida* and YieF and NfsA from *E. coli* as chromate reductases (27, 28). Similarly in 2008, Opperman et al., identified a chromate reductases from *Thermus scotoductus* that exhibited Michealis-Menten kinetics with respect to Cr(VI) (29-31). These proteins were homologous with dihydrolipoamide dehydrogenase and old yellow enzyme; both flavin-dependent enzymes. Later in 2010, it was reported that FerB a homodimeric flavoprotein from *Paracoccus denitrificans* catalyzed the reduction of chromate using NADH as an electron donor(32). Soon after in 2012, Eswaramoorthy et al., published the structure of a flavin dependent quinone reductase, ChrD from *E. coli* that was indicated to have

chromate reducing capacity (33). In 2013, *E. coli* NemA (the flavin dependent N-ethylmaleimide reductase) was also reported to efficiently reduce chromate and described the enzyme as a chromate reductase (34). Later in 2015, Deng et al., claimed chromate reductase activity for the *Serratia* sourced ChrT protein which has high sequence identity with FMN reductase enzymes (35). Lipoamide dehydrogenase activity was shown for a claimed chromate reductase from *Leucobacter* sp. in 2016 by Sarangi and Krishnan (36). Then in 2017, Han et al., reported that the purported chromate reductase activity of NfoR was enhanced in the presence of Cu(II) ions (6). NfoR is the subject of the current investigation, and is clearly similar to known FMN reductase enzymes (Figures 6 & 7).

All proteins described to date as chromate reductases have either a flavin cofactor or use a flavin as a substrate. This is of some importance with regard to enzymatic catalysis of chromate reduction. Early and later reports acknowledged the facile nature of reduction of chromate by reduced flavins (25, 28). Flavins have reduction potentials around -200 mV, almost 1500 mV below that of chromate. Moreover, the redox versatility of the reduced isoalloxazine ensures facile one-electron reactions with metal ions (Figure 10). As such the principal question is whether chromate reduction is catalyzed directly on the surface of these enzymes, fulfilling the chromate reductase definition or if it is a collision-based reaction with bound or free reduced flavin that is not an intended function of these enzymes. It is interesting to note that no structures of putative chromate reductases have been reported that have chromate bound.

The formal definition of a catalyst is an entity that accelerates the rate of a reaction but is itself unchanged by the reaction. Given that all claimed chromate reductases utilize reduced flavins, a fundamental requirement is that they increase the rate of reduction of chromate

relative the rate of reduction by unliganded reduced flavin. This criterium has not yet been met and/or measured in any of the published works that claim to have discovered chromate reductase activity. That no crystal structures have yet been solved with chromate bound does not by itself prove that these enzymes do not harbor this activity. While binding is a consistent property of enzymes, the binding of a substrate is not required for protein to be an enzyme and validated substrates can react in a bimolecular manner with enzymes, such as the reaction of dioxygen with numerous oxygenases (37-39). Michaelis-Menten kinetics are also offered as evidence of enzymatic behavior, however such observations can be deceptive as hyperbolic dependencies arise when some other contingent chemical step becomes rate limiting at high reactant concentrations. In this instance, if the rate of chromate reduction by bound or liberated $FMNH_2$ is substantially less than the rate of flavin reduction and/or release, the observed rate of reaction will approach a limit and thus appear to display conventional Michaelis-Menten kinetics. The only means to formally demonstrate catalysis is direct comparison of catalyzed and uncatalyzed rates. In the absence of such evidence, the existence of chromate reductase activity is unproven. It is interesting to note that well before the first claims of chromate reductase activity, a similar dearth of fundamental evidence had been noted for enzymes miss-categorized as ferric reductases that were in fact also flavin reductases (40).

In 2017, Han et al., showed that RNA for NfoR production is upregulated under chromate induced stress, raising the possibility that increased flavin reduction is a viable strategy to survive chromate rich environments. Here we identify NfoR as an FMN reductase similar in function and structure to known FMN reductase enzymes. Further, we demonstrate that the fundamental catalysis definition required for the chromate reductase designation is not met by this enzyme.

NfoR has low sequence identity but high structural similarity to the paradigm FMN reductase NfsA (Figure 6 & 7). The apparent slow rate of $FMNH_2$ release (Figure 3B) is a common characteristic of flavin reductases presumably designed to limit autooxidation of free reduced flavin (41-43) that results in the futile loss of reducing equivalents (Figure 8). In the case of NfoR, release of reduced flavin is not necessarily required for redox cycling in the presence of an oxidant (Figure 9 and 4A), as in the case with cupric copper which apparently can react with $FMNH_2$ bound to NfoR ~30-fold more rapidly than the release of $FMNH_2$ (Figure 3B). However, with regard to enhanced bioremediation capacity of microorganisms for chromate pollution, engineering of NfoR to increase the rate constant for of $FMNH_2$ release would seem to be a viable strategy.

Conclusive Remarks

While there is no dispute that bacteria adapt to Cr(VI) in the environment, the observation of chromate reduction does not by itself prove that this process is catalyzed by a chromate reductase. Adventitious reduction of chromate (or other toxic oxidants) by reduced flavin is thermodynamically and kinetically favored. Previous reports of chromate reductase activity do not provide direct evidence for catalysis. That all prior reports of chromate reductase activity ascribe the function to a recognizable flavin-dependent enzyme, invokes the possibility that non-catalytic chromate reduction is the common observation. The data presented here make a clear case for NfoR functioning as an FMN reductase that can be enlisted by up-regulation to ameliorate chromate toxicity.

References:

1. Zayed AM, Terry N. 2003. Chromium in the environment: factors affecting biological remediation. Plant and Soil 249:139-156.
2. Guertin J. 2005. Toxicity and Health Effects of Chromium, p 215-230, Chromium Handbook. CRC Press, Danvers, MA.
3. Losi ME, Amrhein C, Frankenberger WT, Jr. 1994. Environmental biochemistry of chromium. Rev Environ Contam Toxicol 136:91-121.
4. Thatoi H, Das S, Mishra J, Rath BP, Das N. 2014. Bacterial chromate reductase, a potential enzyme for bioremediation of hexavalent chromium: a review. J Environ Manage 146:383-399.
5. Losi ME, Amrhein C, Frankenberger WT, Jr. 1994. Bioremediation of chromate-contaminated groundwater by reduction and precipitation in surface soils. Journal of Environmental Quality 23:1141-1150.
6. Han H, Ling Z, Zhou T, Xu R, He Y, Liu P, Li X. 2017. Copper (II) binding of NAD(P)H- flavin oxidoreductase (NfoR) enhances its Cr (VI)-reducing ability. Sci Rep 7:15481.
7. Pace NC, Vajdos F, Fee L, Grimsley G, Gray T. 1995. How to measure and predict the molar absorption coefficient of a protein. ProtSci 4:2411-2423.
8. Hefti MH, Milder FJ, Boeren S, ., Vervoot J, Berkel WJ. 2002. A His-tag based immobilization method for the preparation and reconstitution of apoflavoproteins. Biochem Biophys Acta 1619:139-143.
9. Moran GR. 2019. Anaerobic methods for the transient-state study of flavoproteins: The use of specialized glassware to define the concentration of dioxygen. Methods Enzymol 620:27-49.
10. Massey V. The reactivity of oxygen with flavoproteins, p 3-11. *In* (ed), Elsevier,
11. Holzer W, Shirdel J, Zirak P, Penzkofer A, Hegemann P, Deutzmann R, Hochmuth E. 2005. Photo-induced degradation of some flavins in aqueous solution. Chemical Physics 308:69-78.
12. Otwinowski Z, Minor W. 1997. Processing of X-ray diffraction data collection in oscillation mode. Methods Enzymol 276:307-325.
13. Emsley P, Lohkamp B, Scott WG, Cowtan K. 2010. Features and development of Coot. Acta Crystallogr D Biol Crystallogr 66:486-501.
14. Liebschner D, Afonine PV, Baker ML, Bunkoczi G, Chen VB, Croll TI, Hintze B, Hung LW, Jain S, McCoy AJ, Moriarty NW, Oeffner RD, Poon BK, Prisant MG, Read RJ, Richardson JS, Richardson DC, Sammito MD, Sobolev OV, Stockwell DH, Terwilliger TC, Urzhumtsev AG, Videau LL, Williams CJ, Adams PD. 2019. Macromolecular structure determination using X-rays, neutrons and electrons: recent developments in Phenix. Acta Crystallogr D Struct Biol 75:861-877.
15. Massey V, Hemmerich P. 1978. Photoreduction of flavoproteins and other biological compounds catalyzed by deazaflavins. Biochemistry 17:9-16.
16. Tanner JJ, Lei B, Tu SC, Krause KL. 1996. Flavin reductase P: structure of a dimeric enzyme that reduces flavin. Biochemistry 35:13531-9.
17. Carugo O, Djinovic Carugo K. 2005. When X-rays modify the protein structure: radiation damage at work. Trends Biochem Sci 30:213-9.

18. Hersleth HP, Hsiao YW, Ryde U, Gorbitz CH, Andersson KK. 2008. The crystal structure of peroxymyoglobin generated through cryoradiolytic reduction of myoglobin compound III during data collection. Biochem J 412:257-64.
19. Rohr AK, Hersleth HP, Andersson KK. 2010. Tracking flavin conformations in protein crystal structures with Raman spectroscopy and QM/MM calculations. Angew Chem Int Ed Engl 49:2324-7.
20. Pai EF, Schulz GE. 1983. The catalytic mechanism of glutathione reductase as derived from x-ray diffraction analyses of reaction intermediates. J Biol Chem 258:1752-7.
21. Flores A, Perez JM. 1999. Cytotoxicity, apoptosis, and in vitro DNA damage induced by potassium chromate. Toxicol Appl Pharmacol 161:75-81.
22. Mattagajasingh SN, Misra HP. 1996. Mechanisms of the carcinogenic chromium(VI)-induced DNA-protein cross-linking and their characterization in cultured intact human cells. J Biol Chem 271:33550-60.
23. Stearns DM, Kennedy LJ, Courtney KD, Giangrande PH, Phieffer LS, Wetterhahn KE. 1995. Reduction of chromium(VI) by ascorbate leads to chromium-DNA binding and DNA strand breaks in vitro. Biochemistry 34:910-9.
24. Zhitkovich A, Voitkun V, Kluz T, Costa M. 1998. Utilization of DNA-protein cross-links as a biomarker of chromium exposure. Environ Health Perspect 106 Suppl 4:969-74.
25. Puzon GJ, Petersen JN, Roberts AG, Kramer DM, Xun L. 2002. A bacterial flavin reductase system reduces chromate to a soluble chromium(III)-NAD(+) complex. Biochem Biophys Res Commun 294:76-81.
26. Kwak YH, Lee DS, Kim HB. 2003. Vibrio harveyi nitroreductase is also a chromate reductase. Appl Environ Microbiol 69:4390-5.
27. Ackerley DF, Gonzalez CF, Keyhan M, Blake R, 2nd, Matin A. 2004. Mechanism of chromate reduction by the Escherichia coli protein, NfsA, and the role of different chromate reductases in minimizing oxidative stress during chromate reduction. Environ Microbiol 6:851-60.
28. Ackerley DF, Gonzalez CF, Park CH, Blake R, 2nd, Keyhan M, Matin A. 2004. Chromate-reducing properties of soluble flavoproteins from Pseudomonas putida and Escherichia coli. Appl Environ Microbiol 70:873-82.
29. opperman DJ, Heerden E. 2007. A membrane-associated protein with Cr(VI)-reducing activity from Thermus scotoductus SA-01. FEMS Microbiol Letters 280:210-218.
30. Opperman DJ, van Heerden E. 2007. Aerobic Cr(VI) reduction by Thermus scotoductus strain SA-01. J Appl Microbiol 103:1907-13.
31. Opperman DJ, Piater LA, van Heerden E. 2008. A novel chromate reductase from Thermus scotoductus SA-01 related to old yellow enzyme. J Bacteriol 190:3076-82.
32. Sedlacek V, Kucera I. 2010. Chromate reductase activity of the Paracoccus denitrificans ferric reductase B (FerB) protein and its physiological relevance. Arch Microbiol 192:919-26.
33. Eswaramoorthy S, Poulain S, Hienerwadel R, Bremond N, Sylvester MD, Zhang YB, Berthomieu C, Van Der Lelie D, Matin A. 2012. Crystal structure of ChrR--a quinone reductase with the capacity to reduce chromate. PLoS One 7:e36017.

34. Robins KJ, Hooks DO, Rehm BH, Ackerley DF. 2013. Escherichia coli NemA is an efficient chromate reductase that can be biologically immobilized to provide a cell free system for remediation of hexavalent chromium. PLoS One 8:e59200.
35. Deng P, Tan X, Wu Y, Bai Q, Jia Y, Xiao H. 2015. Cloning and sequence analysis demonstrate the chromate reduction ability of a novel chromate reductase gene from Serratia sp. Exp Ther Med 9:795-800.
36. Sarangi A, Krishnan C. 2016. Detoxification of hexavalent chromium by Leucobacter sp. uses a reductase with specificity for dihydrolipoamide. J Basic Microbiol 56:175-83.
37. Entsch B, Ballou DP, Massey V. 1976. Role of oxygenated flavins in the catalytic reaction of p-hydroxybenzoate hydroxylase, p 111-123. *In* 18/0/15 B (ed), Flavins and Flavoproteins. Elsevier, Amsterdam.
38. Johnson-Winters K, Purpero VM, Kavana M, Nelson T, Moran GR. 2003. (4-Hydroxyphenyl)pyruvate Dioxygenase from Streptomyces avermitilis: The Basis for Ordered Substrate Addition. Biochemistry 42:2072-80.
39. Crozier-Reabe KR, Phillips RS, Moran GR. 2008. Kynurenine 3-monooxygenase from Pseudomonas fluorescens: substrate-like inhibitors both stimulate flavin reduction and stabilize the flavin-peroxo intermediate yet result in the production of hydrogen peroxide. Biochemistry 47:12420-33.
40. Fontecave M, Coves J, Pierre JL. 1994. Ferric reductases or flavin reductases? Biometals 7:3-8.
41. Morrison E, Kantz A, Gassner GT, Sazinsky MH. 2013. Structure and mechanism of styrene monooxygenase reductase: new insight into the FAD-transfer reaction. Biochemistry 52:6063-75.
42. Heine T, van Berkel WJH, Gassner G, van Pee KH, Tischler D. 2018. Two-Component FAD-Dependent Monooxygenases: Current Knowledge and Biotechnological Opportunities. Biology (Basel) 7.
43. Sucharitakul J, Chaiyen P, Entsch B, Ballou DP. 2005. The reductase of p-hydroxyphenylacetate 3-hydroxylase from Acinetobacter baumannii requires p-hydroxyphenylacetate for effective catalysis. Biochemistry 44:10434-42.

Tables

Table 1. Crystallographic data collection and model refinement statistics for the NfoR•FNR•NAD^+ complex (PDB ID 7JH4).

Data collection	
Resolution range (Å) (last shell)[a]	50.00 - 2.02 (2.05 - 2.02)
Space Group	C2
***a*, *b*, *c* (Å)**	174.8, 84.8, 107.7
α, β, γ (°)	90.0, 124.3, 90.0
R_{merge}[a,b]	0.048 (0.622)
R_{pim}	0.036(0.516)
$CC_{1/2}$	(0.588)
Total No. of reflections	311343
No. of unique reflections	84335
Completeness (%)[a]	95.9/75.1
Multiplicity	3.7/3.1
⟨ *I*/σ(*I*)⟩[a]	21.6(1.2)
Resolution ⟨ *I*/σ(*I*)⟩ = 2 (Å)	2.13
Model Refinement	
R_{cryst}/R_{free} (%)	16.9/20.7
Wilson B-factor (Å^2)	24.8
Number of TLS groups	36
Average B factor (Å^2)[c]	34.6
Protein atoms	34.4
Solvent	38.2
Ligands	25.2
Root-mean-square (RMS) deviations	
Bond lengths (Å)	0.007
Bond angles (°)	0.75
Coordinate error (Å)	0.17
Ramachandran statistics	
Favored/allowed/outliers (%)	96.74/2.71/0.54
Rotamer outliers (%)	0.31
Clash score	8.65

[a]Values in parentheses apply to the high-resolution shell indicated in the resolution row
[b]$R = \sum(||F_{obs}| - \text{scale} \times |F_{calc}||)/\sum|F_{obs}|$.
[c]Isotropic equivalent B factors, including the contribution from TLS refinement

Figure Legends

Figure 1. Kinetic Scheme for the Reductive Reaction of NfoR.

Figure 2. Proposed kinetic mechanism for NfoR in the presence and absence of an external oxidant.

Figure 3. Transient State Reduction of FMN by NfoR. A. The initial reduction of FMN from 0.0012-1 seconds, observed when anaerobic NfoR (6.25 μM) in the presence of 12.5 μM FMN was mixed with a range of anaerobic NADPH solutions: 0, 3.12, 6.25, 12.5, 25, 50, 100, 200 μM. The data were fit globally to the model depicted in Figure 1, assuming that the active enzyme concentration was 6.1 μM and a change in extinction coefficient of 8,800 $M^{-1}cm^{-1}$ for FMN reduction. B. The ensuing reduction of residual FMN from 0.01-200 seconds. The data shown are for 12.5, 25, 50, 100, 200 μM NADPH. The data were fit analytically to Equation 1. Arrows indicate increasing NADPH concentration

Figure 4. Demonstration of the kinetics of NfoR with and without an external oxidant. A. NADPH consumption under aerobic conditions. 1 μM NfoR with 5 μM FMN reacting with 20, 40, 60, 80, 100, 120 μM NADPH in the presence of 250 μM dioxygen as an oxidant observed at 340 nm. B. FMN consumption under anaerobic conditions. 4 μM NfoR in the presence of 150 μM NADPH reacting with 15.4, 16.4, 18.4, 22 μM FMN observed at 450 nm. Both data sets were fit

simultaneously using numerical integration to the model depicted Figure 2. Arrows indicate decreasing concentration for successive assays.

Figure 5. Equillibrium Binding to the NfoR•FMN Complex. A. The binding isotherm for NfoR•FMN complex based on fluorescence emission when 3 μM FMN was titrated with apo-NfoR. The data were fit to Equation 2 that describes the general solution to a quadratic equation added to a straight line that accounts for residual FMN in the apo-NfoR sample. Inset shows the difference emission spectrum of FMN as NfoR was titrated (ascending concentrations are from top to bottom). B. The binding absorption difference spectrum of FMN in the NfoR•FMN complex relative to unbound FMN. FMN (20 μM) was mixed with NfoR to a final concentration of 64 μM. The spectrum of unliganded FMN was then corrected for dilution and subtracted from the spectrum obtained in the presence of NfoR.

Figure 6. Structure comparison of NfsA from *Vibrio harveyi* (grey) and NfoR from *Staphlococcus aureus* (red). The structure of NfoR (PDB ID:7JH4) and NfsA (PDB ID: 2BKJ) were aligned using Pymol (Schrödinger Software). Topology diagrams for NfsA and NfoR are shown to the left of each structure.

Figure 7. Conserved Elements of NfoR Compared to NfsA. **Top.** Clustal alignment of NfoR and NfsA. Conserved residues are indicated using gray shaded boxes. **Bottom.** Comparison of the select active site residues that contact the FMN for NfoR from *Staphlococcus aureus* (PDB ID:7JH4) and NfsA from *Vibrio harveyi* (PDB ID: 2BKJ).

Figure 8. Omit difference maps (F_o-F_c at 3.0 σ) generated by individually omitting FMN (green contour) and NAD^+ (blue contour). A. Depiction of the relative position of the NAD^+ nicotinamide and the FMN difference maps. B. 90° rotation of A. depicting evidence for the two-electron reduced oxidation state of the FMN substrate.

Figure 9. Reoxidation of $FMNH_2$ bound to NfoR Under Anaerobic Conditions. A. NfoR (10 μM final) with FMN (100 μM final) was mixed with NADPH (12 μM final) with chromate (0, 6.26, 12.5, 50, 100, 200 μM) and observed at 450 nm. B. NfoR (10 μM final) with FMN (100 μM final) was mixed with NADPH (12 μM final) with cupric copper (0, 3, 12.5, 25, 100, 200 μM) and observed at 450 nm. These data were not fit analytically or to a comprehensive model. Arrows indicate decreasing concentration of oxidant for successive observations.

Figure 10. Reoxidation of photoreduced FAD. Anaerobic FAD (5 μM final) was photoreduced in the presence of 1 mM methionine using a Xenon arc lamp. The reduced flavin was then mixed with oxidant ($CuSO_4$ or $K_2Cr_2O_7$) and observed at 450 nm. A. Reoxidation in the presence of 40, 80, 160, 320, 640 μM $CuS0_4$. Inset depicts the dependence of the rates observed based on the fit to Equation 3. B. Reoxidation in the presence of 20, 40, 160, 320 μM $K_2Cr_2O_7$ (predominately $CrO_4^=$ at pH 8.0). Inset depicts the dependence of the rates observed based on the fit to Equation 3.

Figures

Figure 1

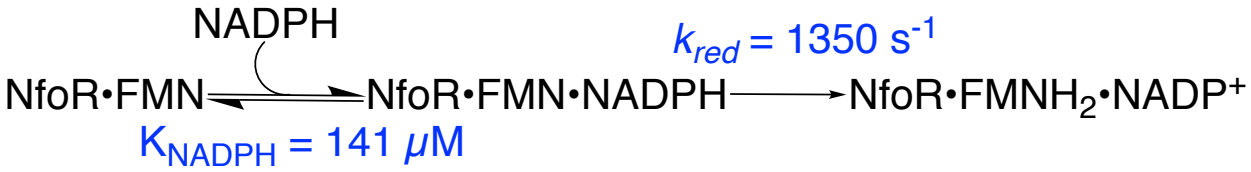

Figure 2.

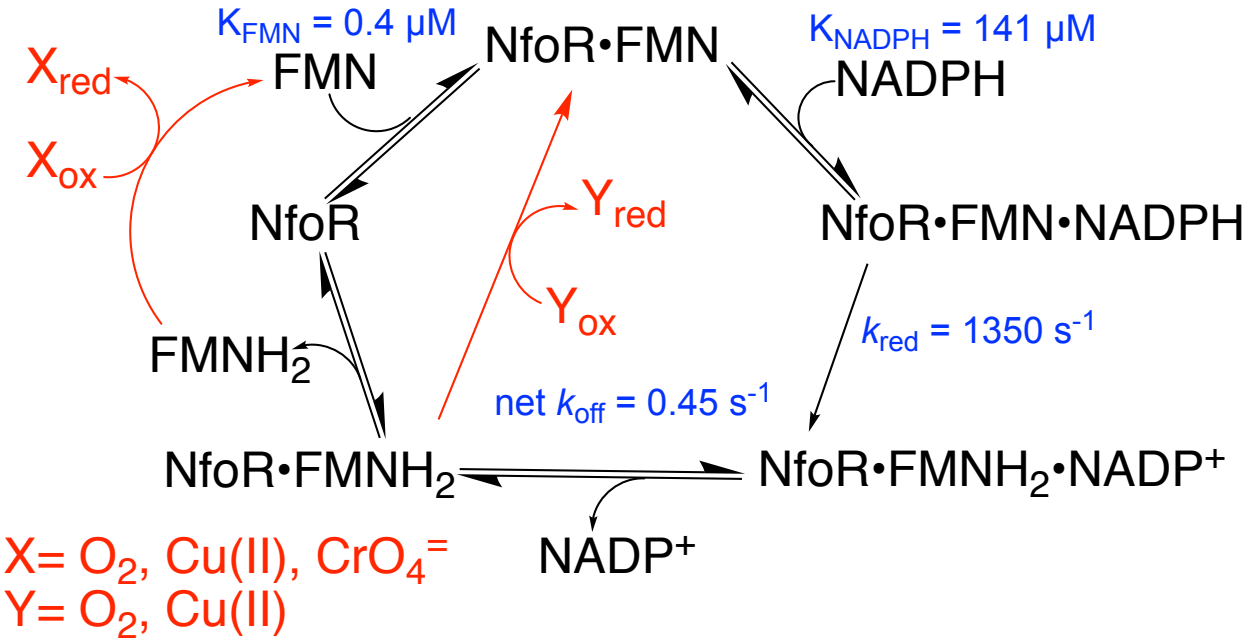
K_{FMN} = 0.4 μM
FMN
NfoR•FMN
K_{NADPH} = 141 μM
NADPH
X_{red}
X_{ox}
NfoR
Y_{red}
Y_{ox}
NfoR•FMN•NADPH
$FMNH_2$
k_{red} = 1350 s^{-1}
net k_{off} = 0.45 s^{-1}
NfoR•$FMNH_2$
NfoR•$FMNH_2$•$NADP^+$
$NADP^+$
X= O_2, Cu(II), $CrO_4^=$
Y= O_2, Cu(II)

Figure 3

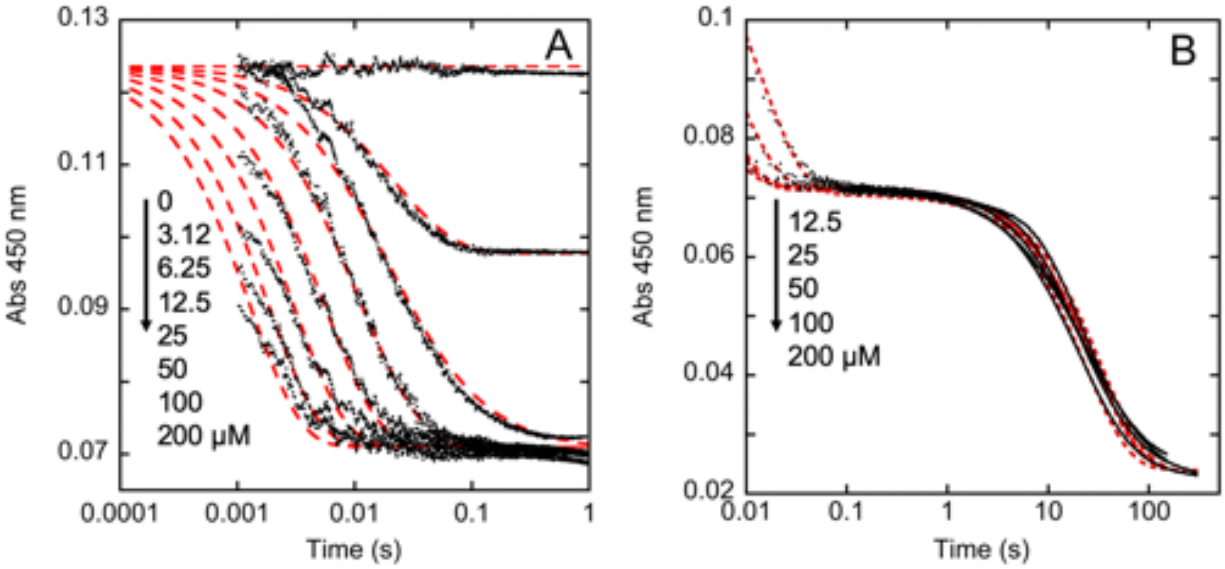
A
0.13
0.11
0.09
0.07
Abs 450 nm
0
3.12
6.25
12.5
25
50
100
200 µM
0.0001
0.001
0.01
0.1
1
Time (s)
B
0.1
0.08
0.06
0.04
0.02
Abs 450 nm
12.5
25
50
100
200 µM
0.01
0.1
1
10
100
Time (s)

Figure 4

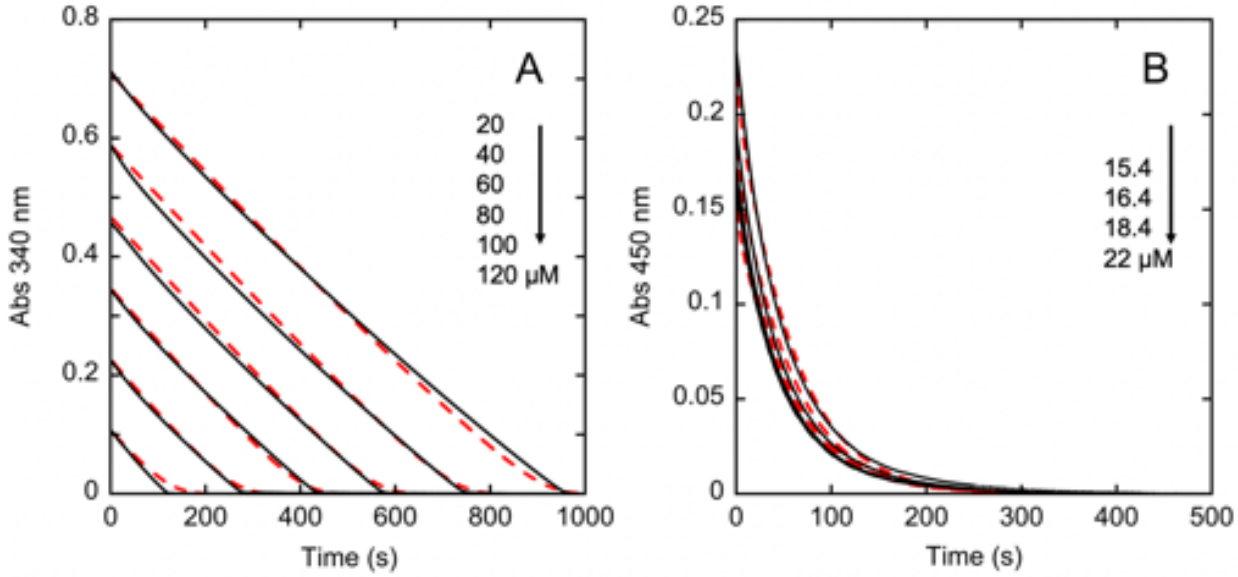
A
Abs 340 nm
Time (s)
20
40
60
80
100
120 µM
B
Abs 450 nm
Time (s)
15.4
16.4
18.4
22 µM

Figure 5.

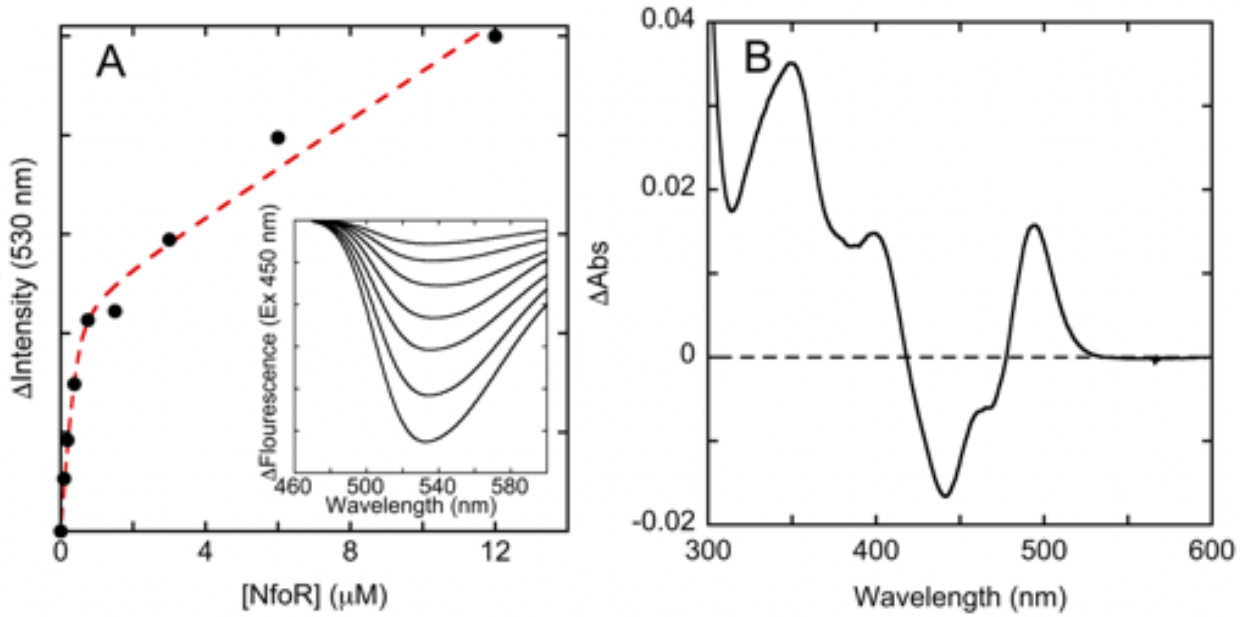
A
ΔIntensity (530 nm)
[NfoR] (μM)
0
4
8
12
ΔFlourescence (Ex 450 nm)
460
500
540
580
Wavelength (nm)
B
ΔAbs
0.04
0.02
0
-0.02
300
400
500
600
Wavelength (nm)

Figure 6.

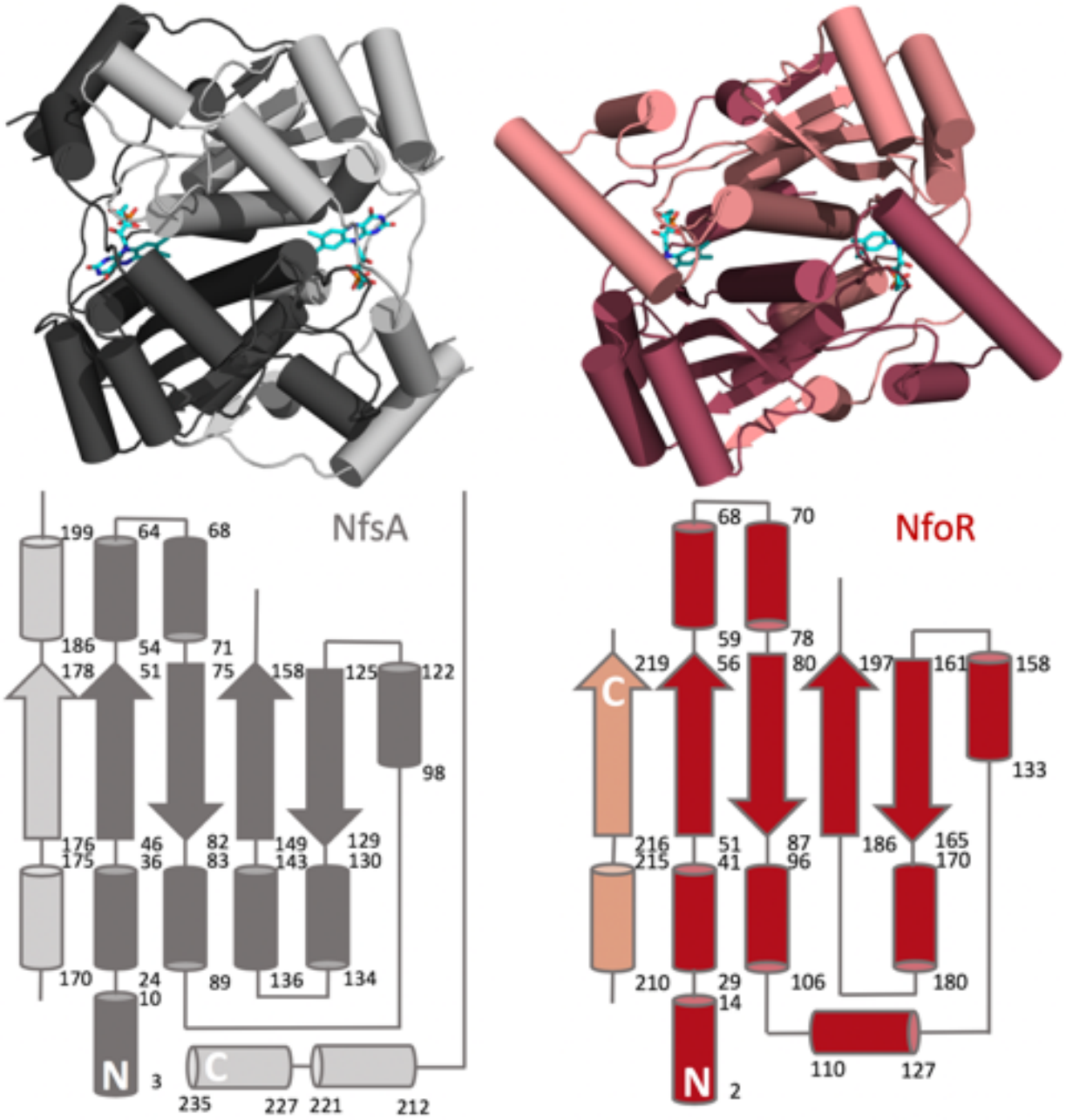
NfsA
199
64
68
186
54
71
178
51
75
158
125
122
98
176
46
82
149
129
175
36
83
143
130
170
24
89
136
134
10
N
3
C
235
227
221
212
NfoR
68
70
59
78
219
56
80
197
161
158
C
133
216
51
87
186
165
215
41
96
170
210
29
106
180
14
N
2
110
127

Figure 7.

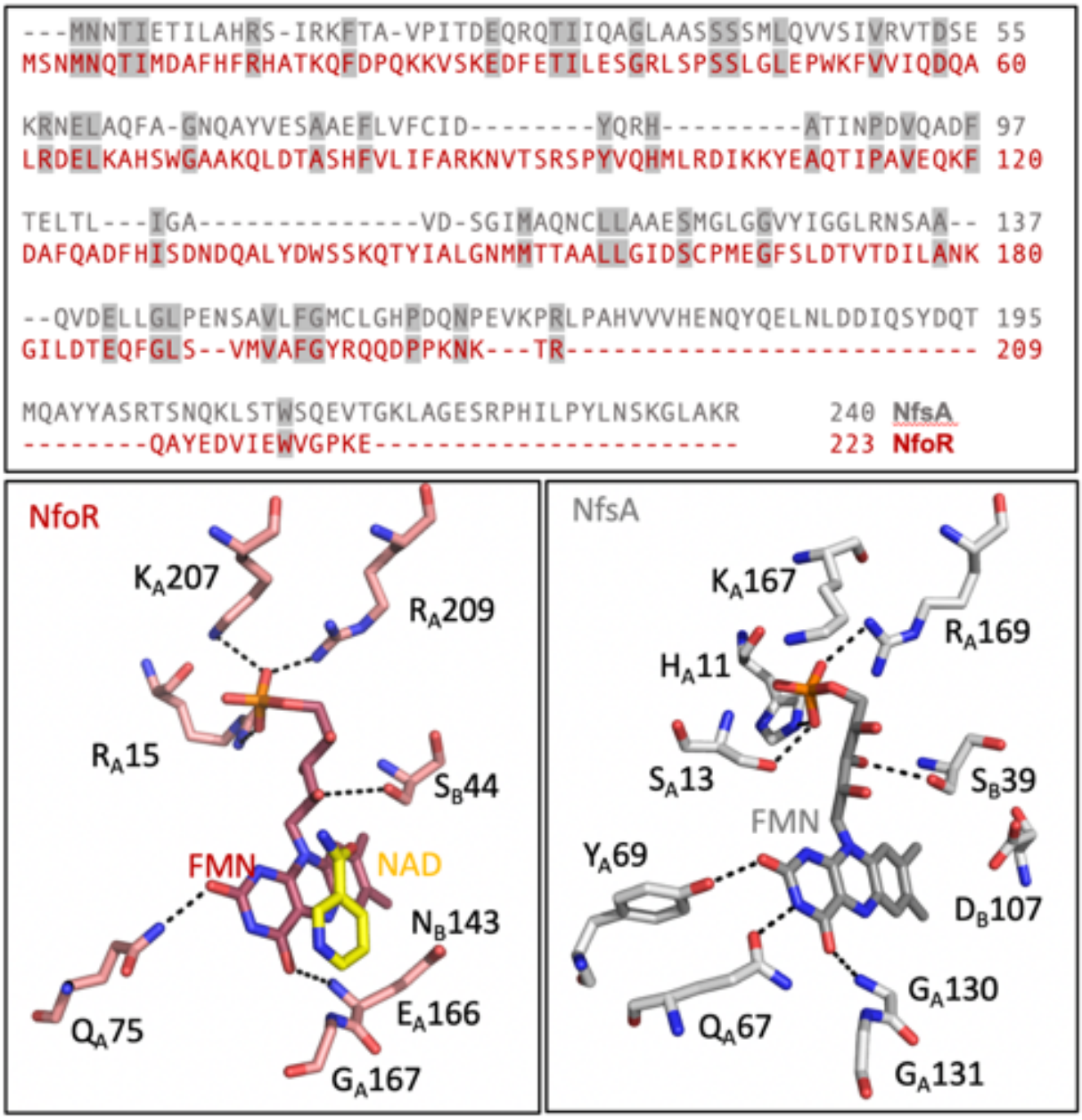
---MNNTIETILAHRS-IRKFTA-VPITDEQRQTIIQAGLAASSSMLQVVSIVRVTDSE 55
MSNMNQTIMDAFHFRHATKQFDPQKKVSKEDFETILESGRLSPSSLGLEPWKFVVIQDQA 60
KRNELAQFA-GNQAYVESAAEFLVFCID--------YQRH---------ATINPDVQADF 97
LRDELKAHSWGAAKQLDTASHFVLIFARKNVTSRSPYVQHMLRDIKKYEAQTIPAVEQKF 120
TELTL---IGA--------------VD-SGIMAQNCLLAAESMGLGGVYIGGLRNSAA-- 137
DAFQADFHISDNDQALYDWSSKQTYIALGNMMTTAALLGIDSCPMEGFSLDTVTDILANK 180
--QVDELLGLPENSAVLFGMCLGHPDQNPEVKPRLPAHVVVHENQYQELNLDDIQSYDQT 195
GILDTEQFGLS--VMVAFGYRQQDPPKNK---TR------------------------- 209
MQAYYASRTSNQKLSTWSQEVTGKLAGESRPHILPYLNSKGLAKR 240 NfsA
--------QAYEDVIEWVGPKE---------------------- 223 NfoR
NfoR
K_A207
R_A209
R_A15
S_B44
FMN
NAD
N_B143
Q_A75
E_A166
G_A167
NfsA
K_A167
R_A169
H_A11
S_A13
S_B39
FMN
Y_A69
D_B107
G_A130
Q_A67
G_A131

Figure 8.

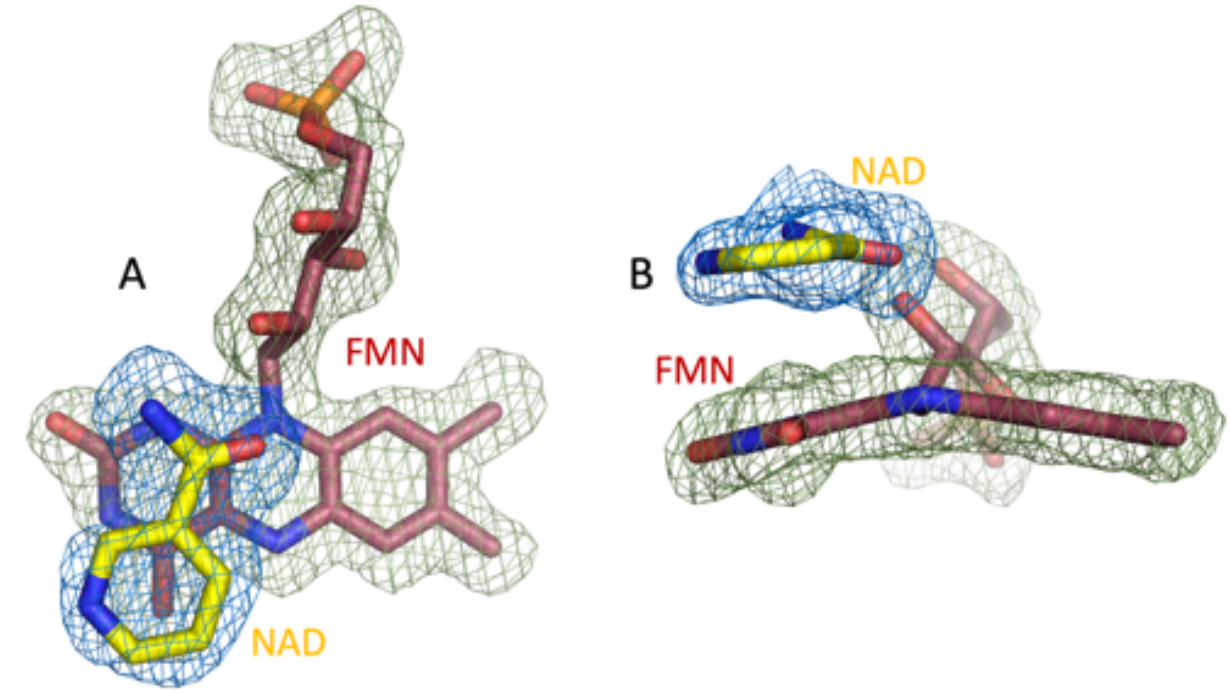

Figure 9.

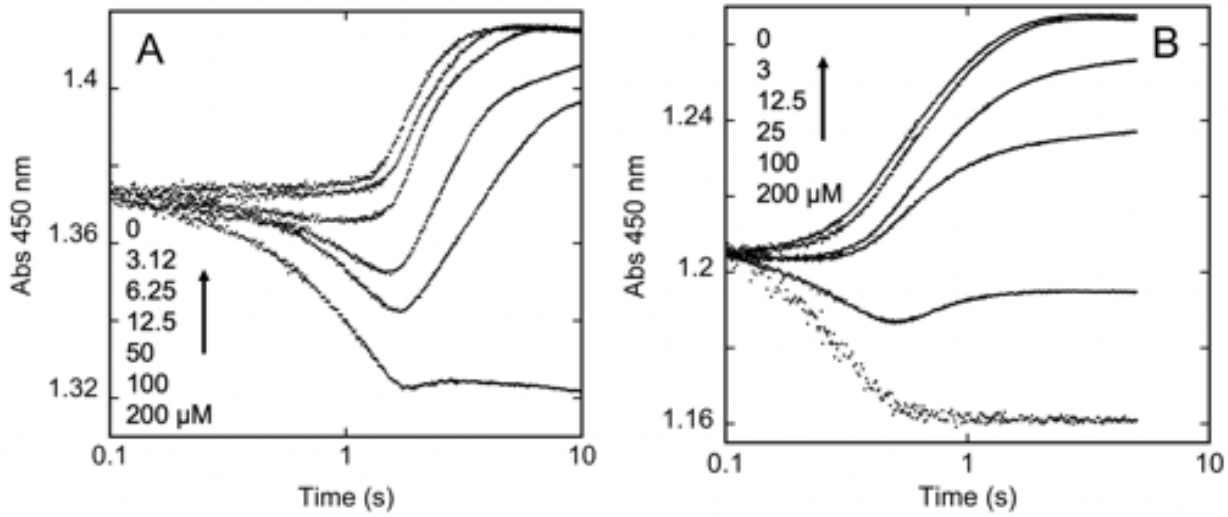
A
1.4
1.36
1.32
Abs 450 nm
0
3.12
6.25
12.5
50
100
200 µM
0.1
1
10
Time (s)
B
1.24
1.2
1.16
Abs 450 nm
0
3
12.5
25
100
200 µM
0.1
1
10
Time (s)

Figure 10.

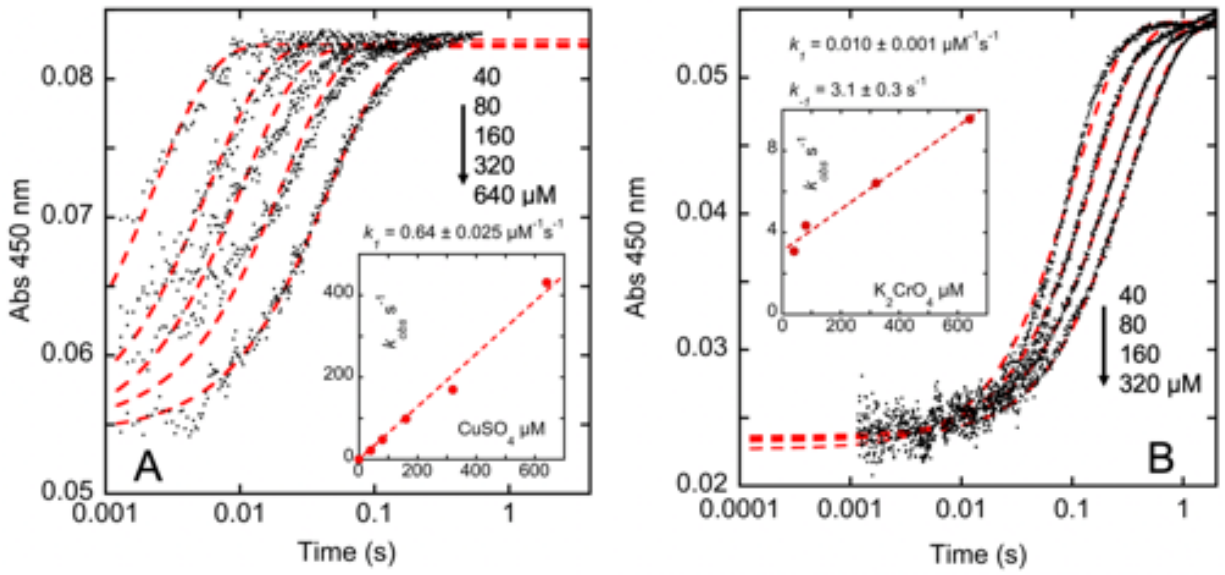
A
Abs 450 nm
Time (s)
40
80
160
320
640 µM
k_1 = 0.64 ± 0.025 µM^{-1}s^{-1}
k_{obs} s^{-1}
CuSO$_4$ µM
B
k_1 = 0.010 ± 0.001 µM^{-1}s^{-1}
k_{-1} = 3.1 ± 0.3 s^{-1}
K$_2$CrO$_4$ µM
40
80
160
320 µM